International Journal of Applied Earth Observation and Geoinformation 134 (2024) 104194

Contents lists available at ScienceDirect

International Journal of Applied Earth Observation and Geoinformation

journal homepage: www.elsevier.com/locate/jag

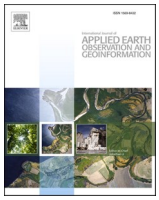

Development of a coral and competitive alga-related index using historical multi-spectral satellite imagery to assess ecological status of coral reefs

Rongyong Huang [a], Zhiwei He [a], Kefu Yu [a,b,*], Zuofang Yao [a,*], Bin Zou [c], Junyou Xiao [a]

[a] Guangxi Laboratory on the Study of Coral Reefs in the South China Sea, Coral Reef Research Center of China, School of Marine Sciences, Guangxi University, Nanning 530004, China
[b] Southern Marine Science and Engineering Guangdong Laboratory (Guangzhou), Guangzhou 511458, China
[c] National Satellite Ocean Application Service, Beijing 100081, China

ARTICLE INFO

Keywords:
Competitive algae
Coral
Coral reef ecosystem
Seasonal dieback
South China Sea

ABSTRACT

Understanding the characteristics of the growth zones of live corals and competitive algae, including turf algae and macroalgae, is crucial for assessing the degradation of coral reef ecosystems. However, identifying live corals and competitive algae in multispectral satellite images is challenging because different objects can have similar spectra. To address this, we used two satellite images acquired at different times (Landsat thematic mapper (TM), Landsat operational land imager (OLI), or Sentinel-2 multi-spectral instrument (MSI)) to assess the growth zone characteristics of live corals and competitive algae. This assessment leveraged the seasonal dieback of competitive algae and the relative stability of live-coral growth zones over a short period. Specifically, we developed a normalized red–green difference index (*NRGI*) to segment live-coral-or-competitive-alga growth zones in satellite images. By comparing the segmentation results from an image captured during a period with few competitive algae and another image captured during a period with lush competitive algae, we estimated the growth zone areas of the live corals and competitive algae. Finally, we calculated the ratio of the competitive-alga growth zone area to the live-coral growth zone area (RCL). Experiments on eight typical coral islands and reefs in the South China Sea (SCS) from 1995 to 2022 revealed that: (1) the identification accuracies of live-coral-or-competitive-alga growth zones reached 80.3 % and 92.6 % during periods with few competitive algae (January to March) and lush competitive algae (April to October), respectively; (2) the RCL was well correlated with the coral-macroalgae encounter rate (an ecological index indicating the pressure of the competitive algae on the live corals) ($r = 0.79$, $P<0.05$); and (3) the trends in the growth zones of competitive algae and live corals, along with the RCL, were consistent with major ecological events in the SCS, such as coral bleaching, outbreak of *Acanthaster planci*, and black band disease. (4) Moreover, a time-lagged correlation was observed between heat stress and the RCL. In summary, the proposed approach is simple, effective, and feasible. The RCL is a valuable indicator of the status of coral reef ecosystems, highlighting the pressure of competitive algae on live corals and the degradation of coral reef ecosystems. This method introduces a novel application of multispectral satellite images for assessing coral reef ecosystems and has significant potential for future coral reef ecosystem monitoring.

1. Introduction

Coral reefs, often referred to as the rainforests of the sea, provide numerous benefits, including seafood, medicines, building materials, and industrial materials. They also play crucial roles in coastal protection, environmental conservation, and sustainable development (Moberg and Folke, 1999). Despite these benefits, coral reefs worldwide are experiencing severe degeneration. For example, the live coral cover (LCC) of the Xisha Islands in the South China Sea (SCS) declined dramatically from 70 % in the 1980 s to 15 % in 2019 (Yu, 2012; Li et al., 2019a). Similarly, in the Caribbean, the LCC decreased from approximately 50 % in the 1970 s to 20 % in 2021 (Gardner et al., 2003; McField et al., 2022). The LCC of the Great Barrier Reef decreased from 28 % to 14 % between 1985 and 2012 (De'Ath et al., 2012). Although recovery

* Corresponding authors at: Guangxi Laboratory on the Study of Coral Reefs in the South China Sea, Coral Reef Research Center of China, School of Marine Sciences, Guangxi University, Nanning 530004, China (K. Yu and Z. Yao).
E-mail addresses: kefuyu@scsio.ac.cn (K. Yu), zfyao@gxu.edu.cn (Z. Yao).

https://doi.org/10.1016/j.jag.2024.104194
Received 23 December 2023; Received in revised form 8 September 2024; Accepted 28 September 2024

was observed in the northern and central parts of the Great Barrier Reef between 2017 and 2022, this recovery was interrupted once again in 2023.

The competition between corals and both turf algae and macroalgae represents a quintessential competitive dynamic within coral reef ecosystems (McCook, 2001). As the LCC decreases, these types of algae often proliferate, subsequently inhibiting coral growth, reproduction, and recovery (Birrell et al., 2005). In many instances, turf algae and macroalgae can even replace corals as the dominant species within the ecosystem (McManus and Polsenberg, 2004).

In this work, turf algae are defined as the heterogeneous assemblages of short filamentous algae (e.g., *Sphacelaria*) and cyanobacteria (e.g., *Synechococcus*) (Fricke et al., 2011). Their presence, along with accumulated sediment, can inhibit the attachment of coral larvae to the seabed (Birrell et al., 2005). Macroalgae, characterized by greater heights, lengths, and biomasses (Liao et al., 2016), are categorized into fleshy macroalgae (e.g., *Asparagopsis*) and calcified macroalgae (e.g., *Halimeda*) (Liao et al., 2021). Corals suffer damage from macroalgae through various mechanisms (River and Edmunds, 2001). For example, macroalgae can release chemosensitive substances that not only reduce coral photosynthesis but also cause coral bleaching and mortality (McCook, 2001; Liao et al., 2016). With the severe decline in the LCC, many coral communities have been gradually replaced by turf algae and macroalgae (Supporting Information, Fig. S1) (Liao et al., 2021). Thus, changes in the growth zones of live corals and competitive algae (including turf algae and macroalgae) can reflect the pressure exerted by algae on live corals and reveal the extent of degradation within coral reef ecosystems.

Unfortunately, shifts between live-coral growth zones and competitive-algae growth zones are primarily assessed via field methods, such as standardized transect or photo quadrat techniques (Chen et al., 2015; Liao et al., 2021). These approaches are time-consuming and labour-intensive. Additionally, the results are limited by the number and distribution of the sampling sites, complicating their application for continuous and large-scale monitoring of coral reefs (Madin and Madin, 2015). Consequently, historical monitoring data on live-coral and competitive-algae growth zones across global coral reefs remain sparse.

Multispectral satellite images offer a valuable technique for observing large-scale areas with high temporal and spatial resolutions. Thus, satellite remote sensing is regarded as a powerful tool for characterizing shifts between live-coral growth zones and competitive-algae growth zones (Huang et al., 2019). However, the spectral reflectances of live corals and competitive algae are remarkably similar in the visible band (the problem of different objects having the same spectrum), complicating their distinction in multispectral satellite images (Hochberg and Atkinson, 2003; Leiper et al., 2011; Chen et al., 2015; Zeng et al., 2020). As a result, many applications either overlook competitive algae in healthy coral reef ecosystems or combine live corals and competitive algae into a single category. For example, the Allen Coral Atlas, a publicly available coral reef map, classifies both under the same category (https://www.allencoralatlas.org/).

Therefore, in this study, we adopted a novel approach by utilizing the seasonal dieback of competitive algae to develop a straightforward index. This index describes the characteristics of live-coral growth zones and competitive-algae growth zones throughout the year, on the basis of multispectral satellite images. Unlike traditional approaches that focus solely on achieving higher classification accuracy, this study emphasizes the importance of the index in reflecting the status of the coral reef ecosystem. Specifically, the main contributions are as follows: 1) A new method to address the challenge of spectral similarity among different objects in remote-sensing analysis, which is specifically tailored to studying the ecological dynamics of coral reefs, is proposed. 2) An innovative concept that integrates the training of both sample classifiers and remote-sensing image classifiers is implemented. 3) The effectiveness of the remote-sensing index in assessing the ecological status of coral reefs is validated. 4) The shifts between live-coral growth zones and competitive-algae growth zones across eight coral reefs in the SCS over the past 25 years are determined. The proposed method provides a crucial foundation for integrating coral reef ecology with remote sensing technology and offers valuable data for understanding the pressure exerted by competitive algae on live corals and the process of coral reef ecosystem degradation.

2. Materials and methods

2.1. Study area

The South China Sea (SCS), the largest semienclosed marginal sea in the northwest Pacific, hosts a critical part of the global coral reef ecosystem. Several coral reefs in the SCS, including Beijiao, Qilianyu, Yongxingdao, Yongle Atoll, Huaguangjiao, Panshiyu, Yuzhuojiao, Langhuajiao, and Huangyandao, have been selected as focal areas (Fig. 1).

2.2. Experimental data

To assess the dynamic changes in live-coral growth zones and competitive-algae growth zones, we utilized a long-term series dataset constructed from Landsat multispectral images (1995–2022) and Sentinel-2 multispectral images (2018–2022). For the Landsat satellites, we employed thematic mapper (TM) and operational land imager (OLI) images, while for the Sentinel-2 satellites, we used multi-spectral instrument (MSI) images. All the images included blue, green, red, and near-infrared bands. The spatial resolution was 30 m for the Landsat TM and OLI images and 10 m for the Sentinel-2 MSI images. In this study, the green and red bands were utilized to construct the Normalized Red-Green Difference Index (*NRGI*). Additionally, a GeoEye-1 true-colour image captured on February 25, 2014, and a WorldView-2 true-colour image captured on October 9, 2014, were used in this study to evaluate the impact of resolution changes on our results. Both images have a resolution of approximately 1.84 m. Prior to feature extraction, the remote sensing reflectances were estimated from these satellite images via traditional preprocessing steps, as illustrated in Supporting Information C. Detailed information regarding the images used is listed in Table S2.

In-situ live coral covers (LCCs) and competitive alga covers (CACs) were used to train a classifier for identifying live-coral growth zones and competitive-algae growth zones in satellite images. Specifically, the source data were obtained from investigative cruises conducted by our team in 2013, 2015, 2021, and 2023. During these cruises, the LCCs and CACs were recorded via a video line intercept transect technique, as detailed in Appendix A of Huang et al. (2018). As shown in Fig. 1, the surveys covered 138 randomly selected in-situ sites: 46 sites were surveyed in 2013, 58 in 2015, 18 in 2021, and 16 in 2023. The 122 pairs of LCCs and CACs from the sites surveyed in 2013, 2015, and 2021 were reported by Chen et al. (2019) and Liao et al. (2021) and were used as the training set in this paper. The LCCs and CACs from the remaining 16 sites surveyed in 2023 were specifically collected to supplement this research and serve as the test set. Furthermore, Chen et al. (2019) interpreted 71 coral-macroalgae encounter rates (CMERs) from videos recorded during investigative cruises, and these rates were also utilized in our discussion. The CMER is an ecological index that reflects the competitive pressure exerted by algae on live corals.

Additionally, remote sensing Sea Surface Temperature-based Degree Heating Week (DHW) is used to indicate accumulated heat stress in a given area over the past 12 weeks (3 months), which can result in coral bleaching and mortality. In this work, the DHW data for the SCS were provided by the National Oceanic and Atmospheric Administration (NOAA) Coral Reef Watch (CRW) (https://coralreefwatch.noaa.gov/product/vs/data.php) and utilized in the discussions.

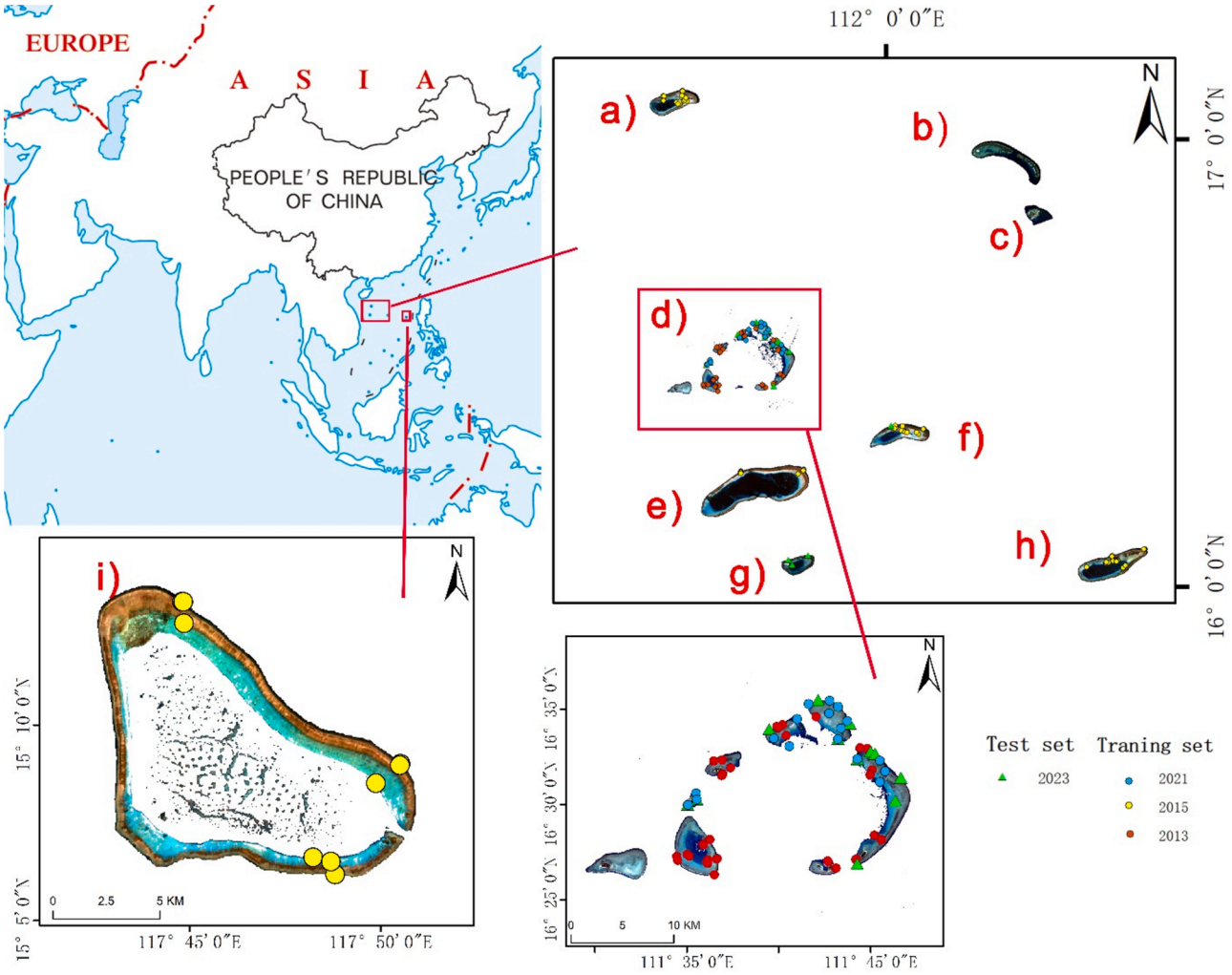

Fig. 1. Distribution of the studied islands and reefs in the South China Sea (SCS): a) Beijiao; b) Qilianyu; c) Yongxingdao; d) Yongle Atoll; e) Huaguangjiao; f) Yuzhuojiao; g) Panshiyu; h) Langhuajiao; and i) Huangyandao. The dots represent the in-situ survey sites. The map in the top left corner was obtained from the Hainan Administration of Surveying Mapping and Geoinformation (http://hism.mnr.gov.cn/). The map number is GS qiong (2023) 040.

2.3. Methods

(1) Construction of a normalized red–green band-difference index (*NRGI*)

On the basis of the seasonal dieback of the competitive algae, we divided a year into two periods: the few-competitive-alga-period and the lush-competitive-alga period. The few-competitive-alga period refers to the months when most competitive algae are dead, and the lush-competitive-alga period refers to the months when the competitive algae are lush. Specifically, for the SCS, the few-competitive-alga period is from January to March, and the lush-competitive-alga period is from April to October. November and December were excluded because they coincide with the gradual decline of competitive algae, placing the algae coverage in a transitional phase between its peak and decline. Moreover, during these months, remote sensing images are frequently obscured by thick clouds due to the transition from the southwest monsoon to the northeast monsoon.

To address the issue of different objects having the same spectrum when distinguishing live-coral growth zones from competitive-algae growth zones (Hochberg and Atkinson, 2003; Leiper et al., 2011; Chen et al., 2015; Zeng et al., 2020), we used the differences between satellite images acquired during these two periods to distinguish these zones throughout a year. To implement this, a normalized red–green band-difference index (*NRGI*) was constructed as follows.

Both live corals and competitive algae contain chlorophyll, which results in high reflection in the green band and strong absorption in the red band (Xu et al., 2019). As demonstrated in Supporting Information Fig. S2, significant differences are observed in the blue–green and red–green bands of the corals. However, Mumby and Edwards (2002) noted that atmospheric Rayleigh scattering affects the red band less than the blue band does. As a result, the contrast between the red and green bands is usually greater than that between the blue and green bands for a satellite image. Additionally, the red band of the Landsat or Sentinel-2 images has a narrower bandwidth than the blue band. Therefore, the red and green bands were chosen to identify live corals and competitive algae. Specifically, the *NRGI* was constructed as follows:

$$NRGI = \frac{G - R}{G + R} \tag{1}$$

where G and R are the reflectances in the green and red bands, respectively.

According to Supporting Information Fig. S2, the *NRGI* values for live corals and competitive algae should be greater than 0. However, previous studies have reported that it is difficult for the red band reflectances of live corals and competitive algae to reach 0 (Zeng et al., 2020). In other words, the *NRGI* values of live corals and competitive algae generally cannot reach 1. For this reason, a threshold T_{NRGI} was set

to identify the live-coral-or-competitive-algae growth zones in the satellite images. Specifically, a pixel was classified as a live-coral-or-competitive-alga growth pixel if and only if the *NRGI* was greater than 0 and less than T_{NRGI}(Criterion ①). Considering that the colour of live coral is strongly influenced by the density of zooxanthellae, which may vary with season and/or temperature, different T_{NRGI} values are set for the few-competitive-alga period and the lush-competitive-alga period.

Taking the estimation of the T_{NRGI} corresponding to the few-competitive-alga-period as an example, we denote the set composed of all the LCCs as $\boldsymbol{S} = \{LCC_1, LCC_2, \cdots, LCC_{122}\}$. Furthermore, we set another threshold for the LCCs, denoted as LCC_T, and defined an in-situ sample as a live-coral-or-competitive-algae growth sample if and only if $LCC > LCC_T$(Criterion ②). Under these conditions, comparisons were conducted using the workflow shown in Fig. 2 to determine the value of T_{NRGI}:

1) Let an intermediate variable $C_i = 2\% + i \times 0.1\%$ (i varies from 0 to 80, or C_i varies from 2 % to 10 % in increments of 0.1 %). For each iteration i, we executed the following steps:

a) We conducted cross-validation via the leave-one-out method. That is, for j varying from 1 to 122, we separated the LCC set $\boldsymbol{S}$ into $\{LCC_j\}$ (test sample set) and $\overline{\boldsymbol{S}}_j = \boldsymbol{S} - \{LCC_j\}$ (training set).

b) We further divided $\overline{\boldsymbol{S}}_j$ into two subsets via Criterion ② with $LCC_T = C_i$: the subset comprising live-coral-or-competitive-algae growth samples was denoted as $\boldsymbol{U}_{i,j}$, and the subset comprising other samples was denoted as $\boldsymbol{V}_{i,j} = \boldsymbol{S} - \boldsymbol{U}_{i,j}$. The *NRGIs* calculated from the satellite images corresponding to $\boldsymbol{U}_{i,j}$ and $\boldsymbol{V}_{i,j}$ were denoted as $\boldsymbol{M}_{i,j}$ and $\boldsymbol{N}_{i,j}$ respectively.

c) We computed the frequency distribution histogram of the *NRGI* within the range of 0–1, using an interval of 0.05 for both $\boldsymbol{M}_{i,j}$ and $\boldsymbol{N}_{i,j}$.

d) We fit the frequency distribution histograms of the *NRGI* for $\boldsymbol{M}_{i,j}$ and $\boldsymbol{N}_{i,j}$ via Gaussian functions and estimated their corresponding Gaussian probability density functions, i.e., $g_{\boldsymbol{M}_{i,j}}(x)$ and $g_{\boldsymbol{N}_{i,j}}(x)$. We denoted their corresponding cumulative distribution functions as $F_{\boldsymbol{M}_{i,j}}(x)$ and $F_{\boldsymbol{N}_{i,j}}(x)$, respectively. Accordingly, if an *NRGI* threshold t was used to identify the live-coral-or-competitive-algae growth zones via Criterion ① with $T_{NRGI} = t$, the error probability for the live-coral-or-competitive-algae growth zones was $1 - F_{\boldsymbol{M}_{i,j}}(t)$, and the error probability for other zones was $F_{\boldsymbol{N}_{i,j}}(t)$.

e) We constructed the following objective function on basis of the principle of minimizing the error probability:

$$L_{i,j}(t) = [1 - F_{\boldsymbol{M}_{i,j}}(t)] + F_{\boldsymbol{N}_{i,j}}(t) \tag{2}$$

f) We solved for the t that corresponds to the minimum of the objective function (2), denoting the solution as $t^*_{i,j}$.

g) We applied $t^*_{i,j}$ to the *NRGI* of the test sample via Criterion ① with $T_{NRGI} = t^*_{i,j}$, and applied C_i to the test sample via Criterion ② with $LCC_T = C_i$.

2) After executing steps a–g for all j with a fixed i, we mimicked the assessment of a classification to compute a quasi-confusion matrix. Specifically, for all j values with a fixed i value, we counted the number of test samples classified into live-coral-or-competitive-algae growth zones via both Criterion ① and Criterion ② in step g ($n^{(i)}_{11}$), the number of test samples classified into nonlive-coral-or-competitive-algae growth zones via both Criterion ① and Criterion ② ($n^{(i)}_{22}$), the number of test samples classified into live-coral-or-competitive-algae growth zones via Criterion ① but classified into nonlive-coral-or-competitive-algae growth zones via Criterion ② ($n^{(i)}_{12}$), and the number of test samples classified into nonlive-coral-or-competitive-algae growth zones via Criterion ① but classified into live-coral-or-competitive-algae growth zones via Criterion ② ($n^{(i)}_{21}$). Thereafter, we computed the quasi-overall accuracy (OA_i) and the quasi-kappa coefficient (K_i) on the basis of the quasi-confusion matrix:

$$OA_i = \frac{n^{(i)}_{11} + n^{(i)}_{22}}{n^{(i)}_{11} + n^{(i)}_{12} + n^{(i)}_{21} + n^{(i)}_{22}} \tag{3}$$

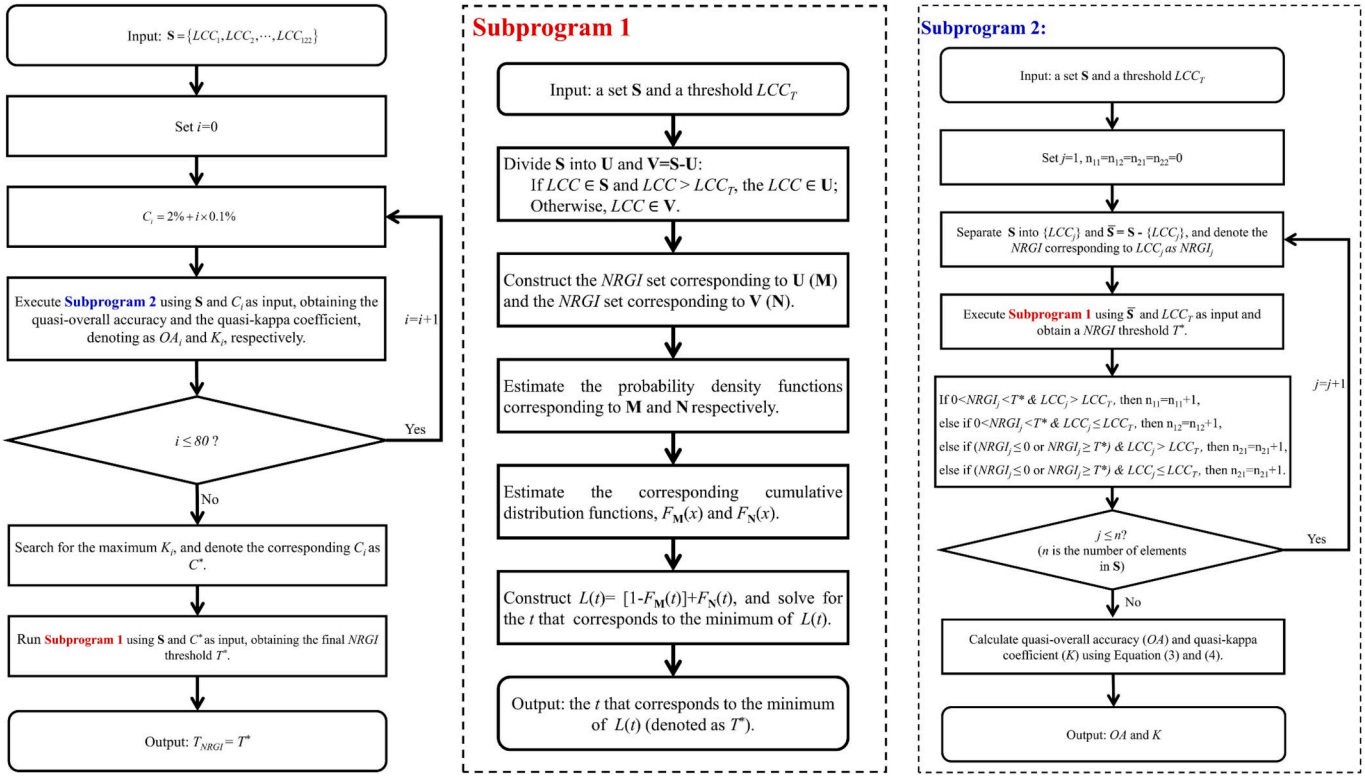

Fig. 2. Program for estimating the threshold T_{NRGI} used to separate the live-coral or competitive-algae growth zones in this study.

$$K_i = \frac{OA_i - E_i}{1 - E_i} \tag{4}$$

where

$$E_i = \frac{[n_{11}^{(i)} + n_{12}^{(i)}][n_{11}^{(i)} + n_{21}^{(i)}] + [n_{12}^{(i)} + n_{22}^{(i)}][n_{21}^{(i)} + n_{22}^{(i)}]}{[n_{11}^{(i)} + n_{12}^{(i)} + n_{21}^{(i)} + n_{22}^{(i)}]^2} \tag{5}$$

3) We searched for the C_i that maximizes the quasi-kappa coefficient K_i and denote the solution as C^*.

4) We re-executed steps b–f by substituting C_i and $\overline{S}_{i,j}$ with C^* and $\boldsymbol{S}$, respectively. The corresponding solution of Equation (2) in step f was used as the final estimated T_{NRGI}.

Note that the T_{NRGI} corresponding to the lush-competitive-alga period was also estimated using the same program, with the LCC set $\boldsymbol{S}$ substituted by $\{LCC_1 + CAC_1, LCC_2 + CAC_2, \cdots, LCC_{122} + CAC_{122}\}$. For convenience, in the following text, the T_{NRGI} corresponding to the few-competitive-alga period is denoted as T_{NRGI}^F, and the T_{NRGI} corresponding to the lush-competitive-alga period is denoted as T_{NRGI}^L.

Once T_{NRGI}^F and T_{NRGI}^L are determined, they can be fixed. In other words, it is unnecessary to repeat steps 1–4 in practical applications; we can simply apply the T_{NRGI}^F and T_{NRGI}^L determined in this paper to other Landsat or Sentinel-2 multispectral images. Another point is that although the interval of the histogram in step c may impact the shape of the distribution, in our experiments, we observed that the estimated $t_{i,j}^*$ values in step f were very similar to each other when we set the interval to 0.03, 0.04, 0.05, 0.06, and 0.07.

(2) Estimation of the characteristics of the growth zones of live corals and competitive algae

Competitive algal growth exhibit significant seasonal dieback (Ferrari et al., 2012; Low et al., 2019; Luo, 2019), whereas coral growth shows minimal seasonal variation unless impacted by ecological disasters, such as mass coral bleaching and mortality (Roff, 2020). In other words, live-coral growth zones should not expand or shrink significantly within a year. For this reason, after T_{NRGI}^F and T_{NRGI}^L were determined via the program shown in Fig. 2, the approach used to estimate the characteristics of the live-coral growth zones and competitive-algae growth zones can be summarized as shown in Fig. 3. The exclusions of deep-water areas, above-water areas, and underwater sand areas from the satellite image shown in the figure were achieved through several traditional methods (Supporting Information D).

For convenience, we denoted the set of live-coral growth pixels obtained by applying T_{NRGI}^F to a few-competitive-alga-period *NRGI* image as $\boldsymbol{C}$ and the set of live-coral-or-competitive-algae growth pixels obtained by applying T_{NRGI}^L to the corresponding lush-competitive-alga-period *NRGI* image as $\boldsymbol{S}$. In addition, we further assigned the set of live-coral growth pixels from the lush-competitive-alga period to the next few-competitive-alga period as $\boldsymbol{E}$, that is, we can apply T_{NRGI}^F to an *NRGI* image during the next few-competitive-alga period to obtain $\boldsymbol{E}$.

According to the analysis described in Supporting Information E, the program used to extract the characteristics of the live-coral growth zones and competitive-algae growth zones shown in Fig. 3 can be implemented via the following steps:

1) We estimated the *NRGI* images from the satellite images during the few-competitive-alga period and the lush-competitive-alga period in a year, according to Equation (1).

2) We obtained $\boldsymbol{C}$ and $\boldsymbol{S}$ by applying the determined T_{NRGI}^F and T_{NRGI}^L to the *NRGI* images respectively.

3) We took the set of live-coral growth pixels as $\boldsymbol{R} = \boldsymbol{C}$.

4) We calculated an intermediate index *Rr* as follows:

$$Rr = \frac{|\boldsymbol{C} - \boldsymbol{S}|}{|\boldsymbol{C}|} \times 100\% \tag{6}$$

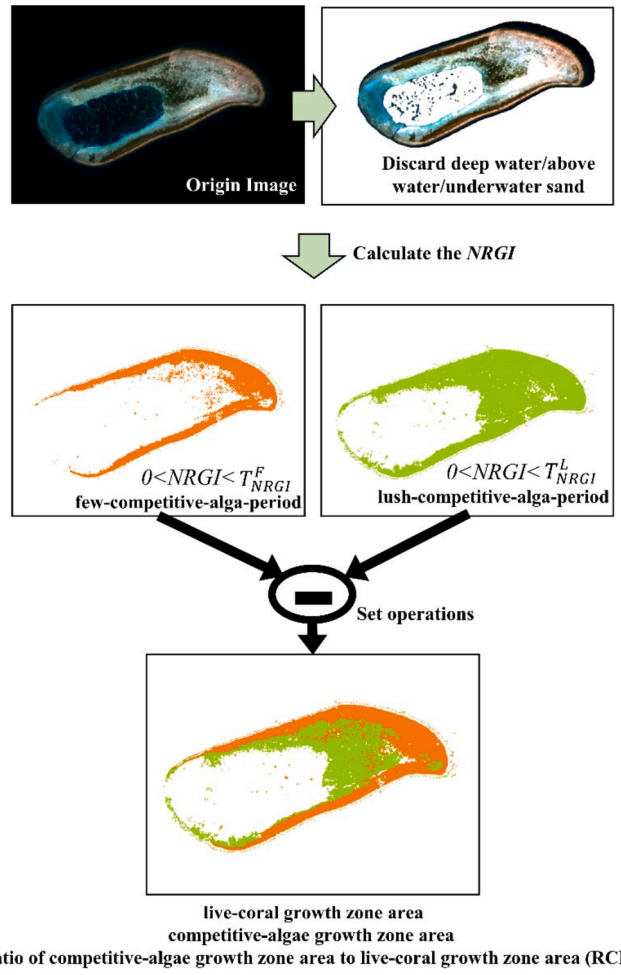

Fig. 3. Schematic diagram illustrating the method used to identify the growth zones of live corals and competitive algae.

5) If *Rr* was less than a given value of T_{Rr}, we took the set of competitive-algae growth pixels as $\boldsymbol{A} \approx \boldsymbol{S} - \boldsymbol{C}$ and skipped to step 7; otherwise, we proceeded to the next step.

6) We obtained $\boldsymbol{E}$ by applying T_{NRGI}^F to the corresponding *NRGI* image and designating the set of competitive-algae growth pixels as $\boldsymbol{A} \approx \boldsymbol{S} - \boldsymbol{E}$.

7) We estimated the growth zone characteristics of the live corals and competitive algae as follows:

$$\begin{cases} S_{\boldsymbol{R}} = |\boldsymbol{R}| \times \Delta^2 \\ S_{\boldsymbol{A}} = |\boldsymbol{A}| \times \Delta^2 \\ R_S = \dfrac{S_{\boldsymbol{A}}}{S_{\boldsymbol{R}}} \times 100\% = \dfrac{|\boldsymbol{A}|}{|\boldsymbol{R}|} \times 100\% \end{cases} \tag{7}$$

where $S_{\boldsymbol{R}}$, $S_{\boldsymbol{A}}$, R_S, and Δ are the live-coral growth zone area, the competitive-algae growth zone area, the ratio of the competitive-algae growth zone area to the live-coral growth zone area (RCL), and the pixel size of the image, respectively.

It should be additionally noted that *Rr* (Equation (6)) was used to determine whether a mass coral bleaching or mortality event is highly likely to occur, thereby deciding whether to execute step 6. According to the reef refuge hypothesis, the probability of coral bleaching caused by high temperatures decreases with increasing latitude (Riegl and Piller, 2003). On the basis of this, the *Rr* value of Beijiao in 2016 was selected as the T_{Rr} value for use in this study, as a global coral bleaching event occurred during 2016 (Supporting Information, Table S1) and Beijiao has the highest latitude in the study area, that is, $T_{Rr} = 2.45\%$. To test the performance when the above T_{Rr} was used, we mimicked

classification accuracy assessment to construct a quasi-confusion matrix by comparing the coral bleaching or mortality events identified via T_{Rr} with the ecological events listed in Table S1 of the Supporting Information. The results showed that the coral bleaching or mortality events determined by using T_{Rr} were highly consistent with the observed events, with a quasi-overall accuracy of 83.6 % and a quasi-kappa coefficient of 0.66, verifying the feasibility of setting $T_{Rr} = 2.45\%$ in the proposed approach.

3. Results

3.1. Growth zones of live corals and competitive algae

Using the LCC and CAC values obtained from the field surveys (the training set shown in Fig. 1) and the satellite images shown in Table S3 of the Supporting Information, we determined the following: 1) $T^{F}_{NRGI} = 0.295$ and $T^{L}_{NRGI} = 0.400$; 2) LCC_T values were 3.3–4.5 % for the few-competitive-alga period and 2.9–3.4 % for the lush-competitive-alga period; and 3) the quasi-overall accuracies were 80.3 % for identifying the live-coral growth zones during the few-competitive-alga period and 92.6 % for identifying the live-coral-or-competitive-algae growth zones during the lush-competitive-alga period (Table 1).

Furthermore, our team investigated 16 survey sites in 2023, the distribution of which is shown in Fig. 1. The obtained LCCs and CACs were used as a test set to further assess the accuracy. The results revealed an overall accuracy of 86.7 % and a kappa coefficient of 0.67 for identifying the live-coral growth zones during the few-competitive-alga period, and an overall accuracy of 93.3 % and a kappa coefficient of 0.64 for identifying the live-coral-or-competitive-algae growth zones during the lush-competitive-alga period.

Additionally, it is important to note that the trained LCC_T was very close to that of Duan (2022), who used an LCC threshold of 3 % to identify live-coral growth zones in the Xisha Islands in the South China Sea (SCS). This provides further evidence of the effectiveness and correctness of the concept of simultaneously training a sample classifier and a remote-sensing image classifier.

In addition, the red and green bands were identified as the optimal band pair for constructing a normalized difference index via Landsat or Sentinel-2 images. As shown in Table 1, both the quasi-kappa coefficient and the quasi-overall accuracy of the proposed *NRGI* were greater than those of the other band pairs.

The live-coral growth zones and competitive-algae growth zones were identified via the thresholds T^{F}_{NRGI} and T^{L}_{NRGI} through the program shown in Fig. 3. One of the results is shown in Fig. 4 (other results are shown in Figs. S5–S11). The live-coral growth zones dominated the reef flats in the SCS before 2007, with some live corals even growing on parts of the lagoon slopes. However, the competitive algae significantly expanded after 2009. As the live-coral growth zones in the reef flats narrowed, competitive algae began to grow in these areas. Additionally, the lagoon slopes started to be covered by a substantial number of competitive-algae growth areas.

To further verify the consistency between the results obtained from the Landsat images and Sentinel-2 images, the live-coral growth zones and competitive-algae growth zones extracted from the Landsat 8 and Sentinel-2 images were compared. The satellite images that were utilized are listed in Table S4 of the Supporting Information. As shown in Fig. 5, the extracted live-coral growth zone and competitive-algae growth zone areas were distributed around the 1:1 line, with a correlation coefficient (r) of 0.998. Using the method described by Huang et al. (2018) to estimate the mean relative error (MRE), the MRE of the areas extracted from Landsat 8 compared with those from Sentinel-2 was approximately 8.0 %. Similarly, the ratio of the competitive-algae growth zone area to the live-coral growth zone area (RCL) was also distributed around the 1:1 line ($r = 0.992$, MRE=8.5 %). Additionally, the live-coral growth zones and competitive-algae growth zones obtained from the Sentinel-2 images were further selected as references to calculate the overall accuracy and kappa coefficient of the results of the Landsat images. The results show that the average overall accuracy and average kappa coefficient were 0.88 ± 0.05 and 0.74 ± 0.09, respectively.

For these reasons, we conclude that the areas extracted via Landsat and Sentinel-2 images were highly consistent, despite their differing resolutions of 30 m and 10 m, respectively. This finding demonstrates that the results from both the Landsat images and the Sentinel-2 images can be reliably used to construct a time series.

3.2. Time series the characteristics of the growth zones of live corals and competitive algae

The time series of the characteristics of the live-coral growth zones and competitive-algae growth zones are shown in Fig. 6. Overall, the area of the live-coral growth zones decreased, whereas the area of the competitive-algae growth zones expanded. Correspondingly, the RCL increased over time. Specifically, the live-coral growth zones experienced three periods of reduction and two periods of recovery. Taking Beijiao as an example, reductions in the live-coral growth zones occurred from 1997 to 1999, 2005–2009, and 2016–2022, with recoveries occurring from 1999 to 2005 and 2009–2015.

To test the sensitivities of satellite data in estimating the live-coral growth zone and competitive-algae growth zone characteristics, we calculated the live-coral growth zone area, the competitive-algae growth zone area, and the RCL of Panshiyu in 2023 by using 12 different combinations of few-competitive-alga period and lush-competitive-alga period images (2 Sentinel-2 MSI images captured in the few-competitive-alga period and 6 captured in the lush-competitive-alga period). The standard deviations of the live-coral growth zone area, the competitive-algae growth zone area, and the RCL were 0.11 km^2, 0.28 km^2, and 0.035, respectively. These standard deviations are much smaller than the variations observed in Fig. 6. Therefore, we conclude that the changes caused by using different few-competitive-alga period or lush-competitive-alga period images can be considered negligible when analysing the changes in coral reef ecosystems via the proposed live-coral growth zone area, competitive-algae growth zone area, and RCL.

Furthermore, the live-coral growth zones and competitive-algae growth zones of Lingyangjiao (16°27′35″ N 111°35′06″ E) in Yongle Atoll were interpreted from the GeoEye-1 image captured on February 25, 2014, and the WorldView-2 image captured on October 9, 2014.

Table 1
Assessments of different band pairs in constructing a normalized difference index for identifying the live-coral-or-competitive-algae growth zones via a Landsat or Sentinel-2 images.

Band Pair		Green–Red (*NRGI*)	Blue–Green	Coastal–Green	Blue–Red	Coastal–Red	Coastal–Blue
FCAP	Quasi-Kappa Coefficient	0.602	0.295	0.344	0.222	0.184	0.396
	Quasi-Overall Accuracy	80.3 %	64.8 %	67.2 %	61.5 %	59.0 %	76.1 %
LCAP	Quasi-Kappa Coefficient	0.701	0.326	0.241	0.467	0.448	0.363
	Quasi-Overall Accuracy	92.6 %	67.2 %	61.5 %	74.6 %	76.2 %	79.3 %

Note: *NRGI*, FCAP, and LCAP are the normalized red–green band-difference index, the few-competitive-alga-period, and the lush-competitive-alga period, respectively. Cross-validation was performed using leave-one-out method, involving a total of 122 validation samples.

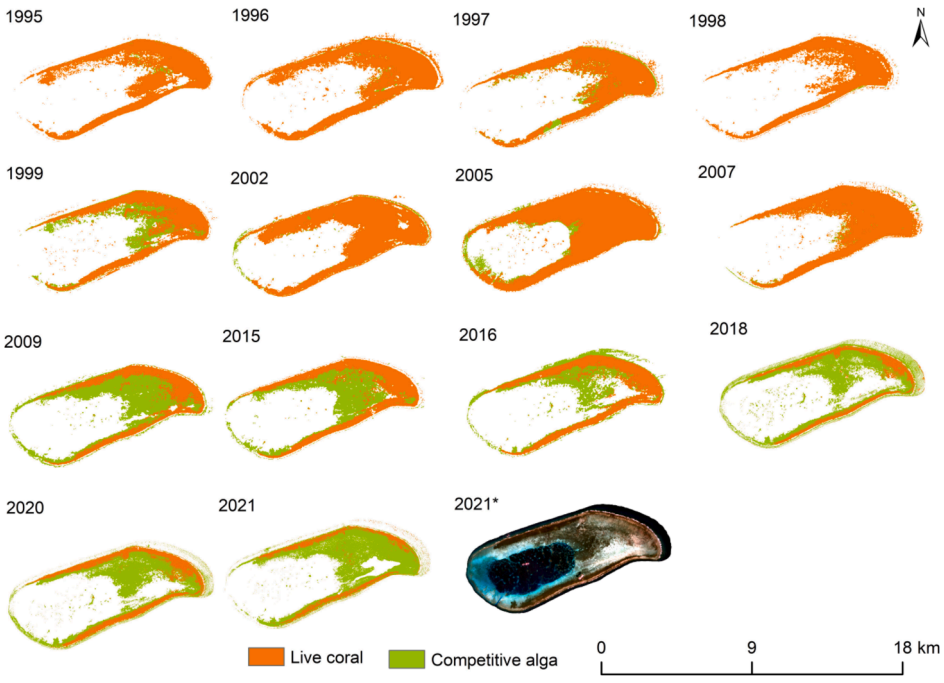

Fig. 4. Growth zones of live corals and competitive algae in Beijiao. * denotes the latest true color image.

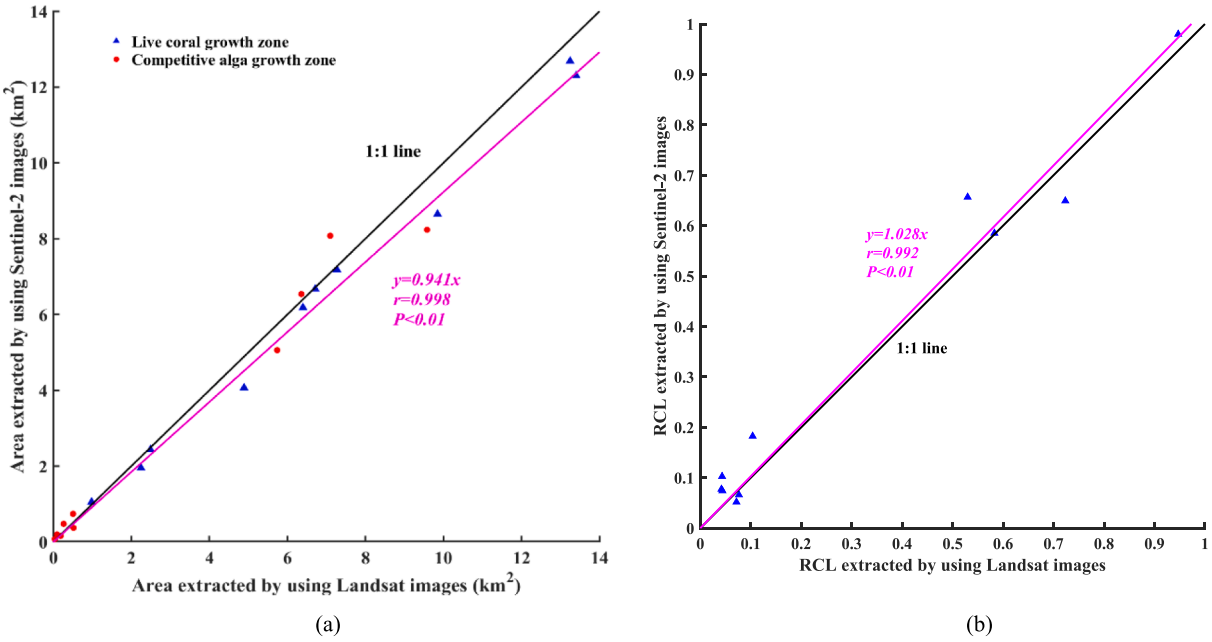

(a) (b)

Fig. 5. Comparisons of the live-coral-or-competitive-algae growth zones extracted from the Landsat 8 images and Sentinel-2 images. (a) Areas obtained from Landsat and Sentinel-2 images and (b) RCLs obtained from Landsat and Sentinel-2 images.

These high-resolution live-coral growth zones and competitive-algae growth zones were used as references to assess the live-coral growth zones and competitive-algae growth zones extracted from Landsat OLI images captured in 2014. The results show that the overall accuracy and the kappa coefficient were 92.7 % and 0.73, respectively, for the few-competitive-alga-period and 90.9 % and 0.82, respectively, for the lush-competitive-alga period. In other words, the live-coral growth zones and competitive-algae growth zones extracted from the 30-m resolution Landsat OLI images were consistent with those from the high-resolution images. In fact, the differences between the live-coral growth zone area, the competitive-algae growth zone area, and the RCL extracted from the high-resolution images and the Landsat OLI images were only 0.28 km^2, 0.41 km^2, and 0.023, respectively.

4. Discussion

4.1. Utilizing the seasonal dieback of competitive algae is reasonable

According to Li et al. (2011a), live corals often expel some of their endosymbiotic zooxanthellae during the lush-competitive-alga period because of the increases in temperature and solar radiation. This usually leads to varying degrees of coral bleaching (Fitt et al., 2000). However,

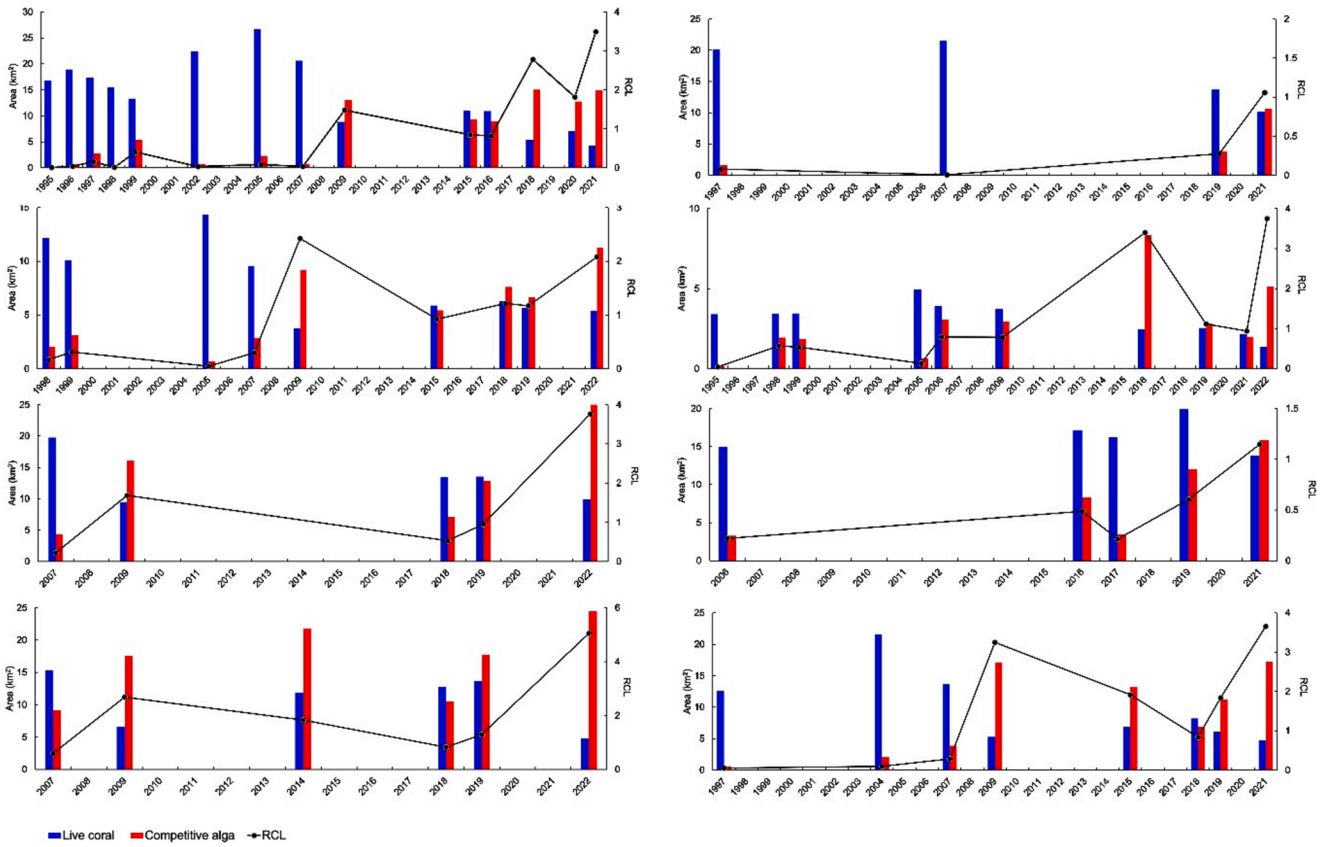

Fig. 6. Time series of the growth zone characteristics of the live corals and competitive algae (the live coral growth area, the competitive algal growth area, and the ratio of the areas of the competitive algae and live coral growth zones): 1) Beijiao; 2) Qilianyu; 3) Panshiyu; 4) Yongxingdao; 5) Huaguangjiao; 6) Huangyandao; 7) Langhuajiao; and 8) Yuzhuojiao.

satellite images often appear darkener, rather than whiter, from the few-competitive-alga period compared with the lush-competitive-alga period (Fig. 7(c) and (e)). This contradiction can be explained by the seasonal dieback of the competitive algae. Moreover, comparisons of the LCC and CAC obtained from the satellite images and the field surveys further illustrate that the darkening from the few-competitive-alga period to the lush-competitive-alga period was caused by the seasonal dieback of the competitive algae in the SCS. The reason for this is that except for the situation shown in Fig. 7(c) and (e), other combinations of the LCCs and CACs do not cause the hue of the image to change from brighter during the few-competitive-alga period to darker during the lush-competitive-alga period (Fig. 7(a), (b), and (d)). In fact, as additional evidence, the darkening of satellite images due to algal growth has also been reported for seagrass beds in the Caribbean Sea (Wabnitz et al., 2008).

Owing to the seasonal dieback of competitive algae, the areas of the live-coral-or-competitive-algae growth zones gradually decreased after October, reaching their minimum values typically between January and March. Taking the Sentinel-2 images of Beijiao and Panshiyu from 2018 to 2019 as examples (detailed information about the utilized images is presented in Table S5 of the Supporting Information), the live-coral-or-competitive-algae growth zones were extracted each month via the proposed *NRGI*. The results, shown in Fig. 8, indicate that in the SCS, the areas of the live-coral-or-competitive-algae growth zones were larger from April to October than in other months. Additionally, the competitive-algae growth zone area in Glover's Reef Atoll, which is located at a similar latitude, has been reported to exhibit a trend of similar seasonal changes (Ferrari et al., 2012).

According to field survey data, common turf algae in the SCS include *Sphacelaria*, *Ectocarpus*, *Feldmannia*, *Hinksia*, *Polysiphonia*, *Gelidiella*, and *Gelidiopsis*. Common macroalgae include *Asparagopsis*, *Dictyota*, *Lobophora*, and *Halimeda*. Notably, except for *Halimeda*, seasonal dieback of these algae occurs in the SCS. On the basis of the interpretation of videos of field survey transects, the average CAC was approximately 7.5 %, with *Halimeda* covering only 0.27 %, accounting for 3.6 % of the competitive algae. Thus, the influence of *Halimeda* on the seasonal dieback of competitive algae can be considered negligible in this study.

In addition, some seagrasses, such as *Halophila ovalis*, are also found in some coral reefs in the SCS, as observed in field survey videos. Fortunately, as shown in Fig. 9, the seagrasses are primarily distributed in the underwater sand in the deep lagoons, where the corresponding satellite image pixels were classified as the deep-water area and excluded in the proposed approach. After these areas were excluded, only 3.3 % of the field survey videos contained seagrasses, with an average coverage of much less than 0.1 %. Therefore, similar to *Halimeda*, the influence of seagrasses on the extraction of the live-coral growth zones and competitive-algae growth zones could also be considered negligible.

For these reasons, we believe that utilizing the seasonal dieback of competitive algae is reasonable; thus, the few-competitive-alga period and lush-competitive-alga period can be defined as January–March and April–October, respectively, in the SCS. Additionally, when sufficient satellite images are available, the set of live-coral growth pixels and the set of live-coral-or-competitive-algae growth pixels can also be determined via the pixels corresponding to the minimum and maximum areas in a year, respectively.

4.2. Competitive-algae growth zone, live-coral growth zone, and their ratio are highly important for indicating the status of a coral reef ecosystem

The areas of live-coral growth zones, competitive-algae growth

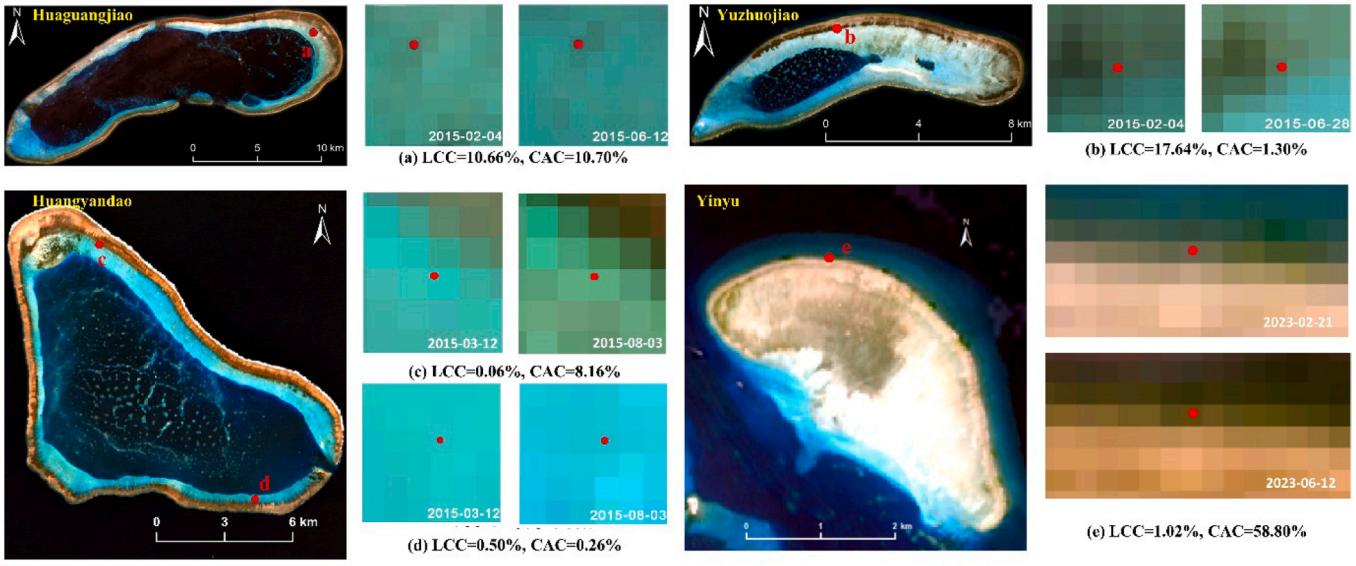

Fig. 7. Examples of seasonal changes in corals and competitive algae in satellite images from the few-competitive-alga period to the lush-competitive-alga period. (A) & (C) Positions of the survey sites (dots), (B) & (D) LCCs and CACs obtained during the field survey and the corresponding Landsat 8 OLI images. (a) When both the LCC and the CAC are much greater than zero (LCC≫0 and CAC≫0), the hues of the image during the few-competitive-alga period and the lush-competitive-alga period are both dark; (b) When the LCC is much greater than zero and the CAC is close to zero (LCC≫0 and CAC→0), the hues of both images are also dark; (c) & (e) When the LCC is close to zero and the CAC is much greater than zero (LCC→0 and CAC≫0), the hues change obviously from bright during the few-competitive-alga period to dark during the lush-competitive-alga period; (d) When both the LCC and the CAC are close to zero (LCC→0 and CAC→0), the hues of the two images are bright. Note that (c) is located on the lagoon slope, where the substrate is predominantly sand, while (e) is on the reef flat, where the substrate is primarily rocky. The differences in substrate composition cause the satellite image of (c) to appear brighter or whiter than that of (e). However, in both cases, the hues shift from relatively bright during the low-competitive-algae period to relatively dark during the lush-competitive-alga period.

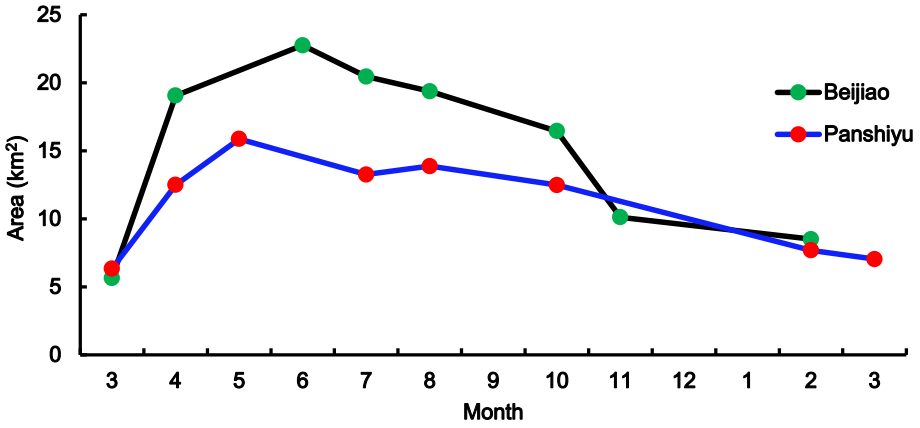

Fig. 8. Results of the month-by-month extraction of the live-coral-or-competitive-algae growth zone areas in Beijiao and Panshiyu.

zones, and their ratio (RCL) can be used to indicate the pressure exerted by competitive algae on live corals and to reveal the extent of degradation within coral reef ecosystems caused by mass coral bleaching or mortality. The details are as follows:

(1) The ratio of the competitive-algae growth zone area to the live-coral growth zone area is strongly correlated with the coral-macroalgae encounter rate

The coral-macroalgae encounter rate (CMER) is a crucial ecological index that indicates the pressure that competitive algae impose on live corals (Chen et al., 2019). As shown in Fig. 10, there is a significant linear correlation ($r = 0.79$, $P<0.05$) between the RCLs and the CMERs reported by Chen et al. (2019). This correlation suggests that the RCL can be used instead of the CMER to indicate the pressure exerted by competitive algae on live corals. An increase in the RCL signifies a greater proportion of competitive algae in the coral reef ecosystem, making the RCL a useful indicator of coral-algal phase shifts in coral reef ecosystems.

(2) The variations in the characteristics of the growth zones of live corals and competitive algae are closely aligned with coral bleaching or mortality events in the SCS

Coral reef degradation is generally caused by mass coral bleaching or mortality, which can result from temperature anomalies, outbreaks of *Acanthaster planci*, and black band disease (De'Ath et al., 2012; Li et al., 2019b). Therefore, we compared the characteristics of the live-coral

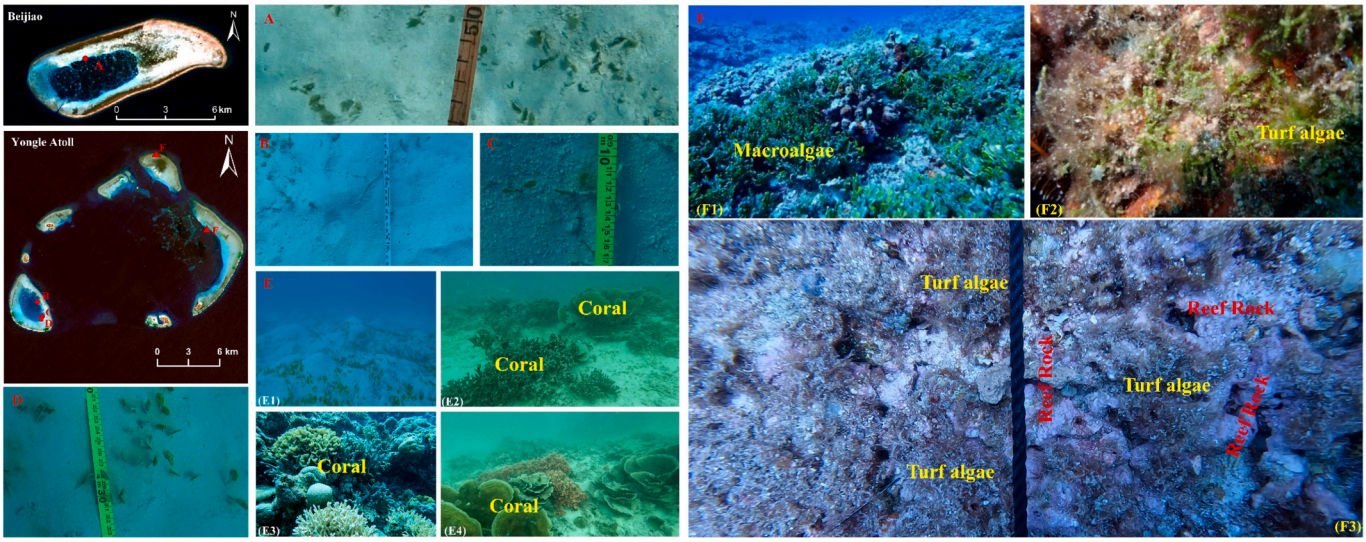

Fig. 9. Seagrass growth in coral reefs in the SCS (several photographs taken at the Beijiao and Yongle Atoll are presented as examples). A, B, C, and D present several frames extracted from the field survey videos (2015). These frames show that the seagrass coverages at the field survey sites were close to zero. E) Several photographs captured during 2022: (E1) seagrasses (*Halophila ovalis*) were observed in the deep lagoon; (E2) only a small number of *Halophila ovalis* were observed in a few transition zones between the coral growth area and the sandy area; (E3) seagrasses were difficult to find in the live-coral growth zones; and (E4) seagrasses were not observed in most of the other transition zones between the coral growth area and the sandy area. F) Photographs of macroalgae (F1) and turf algae (F2) captured during 2023, along with a turf algae frame (F3) extracted from the 2023 field survey video: seagrasses were also difficult to find in the competitive-algae growth zones. On the other hand, according to (F3), there is little sand in the substrate; instead, it is predominantly composed of reef rocks. Additionally, as shown in (F1), (F2), and (F3), the substrate around position F is primarily covered by competitive algae. Notably, position F in this figure corresponds to position e in Fig. 7. According to Fig. 7(D), the CAC around this position is 58.80%, while the LCC is 1.02%.

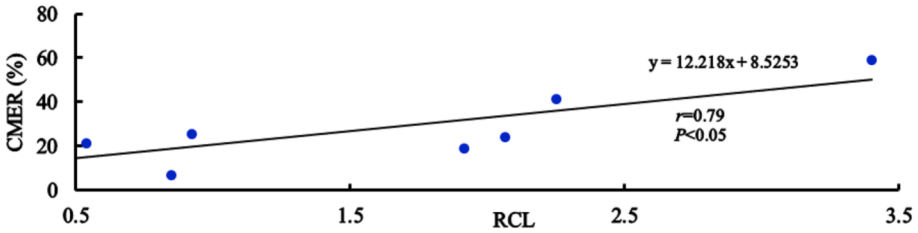

Fig. 10. Correlation between the coral-macroalgae encounter rate (CMER) and the ratio of the competitive-algae growth zone area to the live-coral growth zone area (RCL).

growth zones and competitive-algae growth zones with several typical coral bleaching or mortality events (listed in Table S1 of the Supporting Information). Taking Beijiao as an example, the results are shown in Fig. 11.

The corals in the SCS likely experienced significant mortality following the global coral bleaching events of 1997–1998 and 2015–2016 (Supporting Information, Table S1). Mass coral mortality is usually accompanied by the expansion of competitive algae (Fricke et al., 2011), as these algae can cover the skeletons of dead corals and occupy the available ecological niches (Raymundo and Maypa, 2002). Consequently, except for the decrease in the area of the live-coral growth zones, the area of the competitive-algae growth zones and the RCL increase after a mass coral bleaching event (McCook, 2001). This is consistent with the results presented in Fig. 11.

Furthermore, during the outbreaks of *Acanthaster planci* and black band disease from 2006 to 2009 (Supporting Information, Table S1), the area of the live-coral growth zones decreased, whereas the area of the competitive-algae growth zones and the RCL increased (Fig. 11). This finding aligns with the characteristics of these outbreaks, as both can lead to massive coral mortality (Yang et al., 2014; Li et al., 2019b). *Acanthaster planci* preyed on live corals, directly reducing the live-coral growth zone area. Moreover, competitive algae occupy vacated spaces, expanding their growth zones (Li et al., 2019b). Similarly, black band disease exposes coral skeletons, which are then rapidly covered by competitive algae, further increasing the area of the competitive-algae growth zones (Huang and Yu, 2010; Yang et al., 2014).

In addition, the average LCC of coral reefs in the Xisha Islands decreased from more than 60 % before 2006 to less than 5 % in 2011 because of simultaneous outbreaks of *Acanthaster planci* and black band disease from 2006 to 2009 (Li et al., 2019a). This decrease was much more significant than that observed during the mass coral bleaching event of 1997–1998. As shown in Fig. 11, the decrease in the live-coral growth zone area and the increases in the competitive-algae growth zone area and the RCL were much greater from 2006 to 2009 than from 1997 to 1999. Once again, this is consistent with the dramatic decline in the LCCs.

Similarly, as shown in Table S1 of the Supporting Information, the density of *Acanthaster planci* in Beijiao was 0.0017 ind./m^2 in 2020, which barely exceeded the tolerable limit of 0.0015 ind./m^2; this indicates that the outbreak of *Acanthaster planci* in Beijiao began in 2020. This outbreak also corresponds well with the decline in the area of the live-coral growth zones and the increases in the area of the competitive-algae growth zones and the RCL from 2020 to 2021 (Fig. 11).

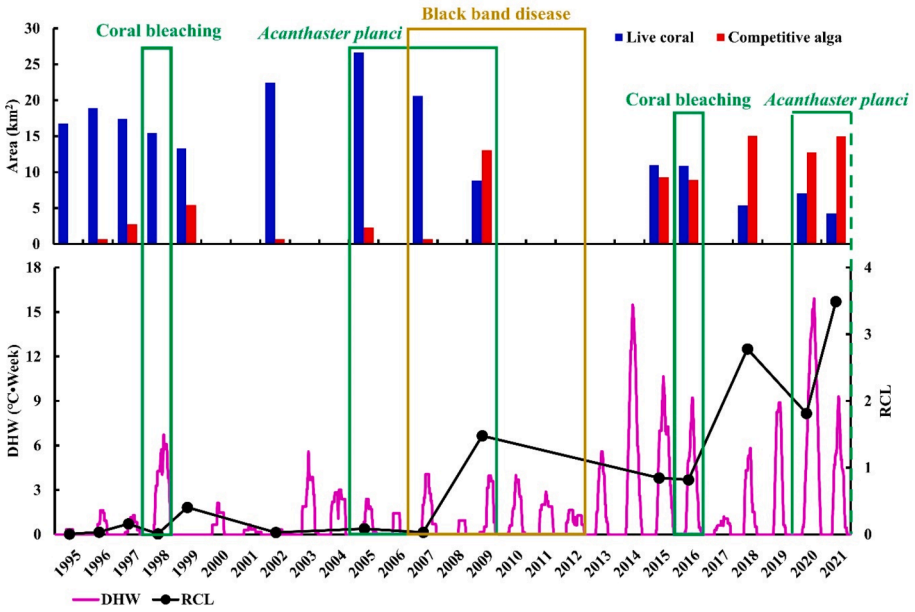

Fig. 11. Comparisons among typical coral bleaching or mortality events, the characteristics of live-coral and competitive-algae growth zones, and heat stress in the Xisha Islands of the SCS (using Beijiao as an example). The latest outbreak of *Acanthaster planci* in the Xisha Islands began in 2018–2019, and its end has not yet been reported (Supporting Information, Table S1).

(3) The variations in the characteristics of the live coral and competitive algae growth zones are consistent with the recovery periods of the coral reefs

In addition to the ecological disaster events, two typical coral reef recovery periods in the SCS that were observed in this study were also consistent with historical ecological survey data. According to surveys conducted by Huang et al. (2011), the coral reefs in the SCS are dominated by branched corals. Branched corals can grow quickly and are considered the cornerstone of coral reef recovery (Wilson et al., 2019). In fact, surveys conducted by Li et al. (2011b) in 2007 revealed a batch of newly grown branched corals in the SCS only 10 years after the 1997–1998 coral bleaching event. Importantly, the ages of most of these corals were less than 10 years. Therefore, the coral reefs in the SCS experienced a recovery period from 1999 to 2006. This conclusion is quite consistent with the variations in the characteristics of the live-coral growth zones and competitive-algae growth zones shown in Figs. 6 and 11.

Furthermore, field surveys have shown that the LCC values of coral reefs in the SCS increased from 7.93 % in 2009 to 16.3 % in 2015 (Wu et al., 2011; Chen et al., 2019). This increase indicates that coral reef ecosystems slowly recovered from 2009 to 2015, which corresponds well with the expansions of the live-coral growth zones shown in Figs. 6 and 11. However, the fact that the LCC reached only 16.3 % indicates that the coral reef ecosystems were still unhealthy. Additional evidence of the unhealthy state was observed in the CAC of Yongxingdao, which was approximately five times greater than the LCC (40.25 % V.S. 6.46 %) in 2015 (Luo, 2019), whereas the LCC in Yongxingdao was as high as ~ 90 % in the 1980 s (Yu, 2012). The unhealthy state of these coral reef ecosystems is supported by changes in the RCL (Figs. 6 and 11). Although the RCL decreased as the coral reef ecosystems recovered, it remained greater than 1, indicating the continued unhealthy state of the ecosystems.

(4) Time-lagged correlation of heat stress with the ratio of the competitive-algae growth zone area to the live-coral growth zone area

Heat stress is considered one of the major factors contributing to coral degradation (De'Ath et al., 2012; Li et al., 2019a, 2019b). The degree heating week (DHW) index can be used to assess accumulated heat stress, which can lead to coral bleaching and mortality. Once coral death occurs, competitive algae are likely to occupy the positions of the dead corals in the subsequent period. This means that the ratio of the competitive-algae growth zone area to the live-coral growth zone area (RCL) should not increase simultaneously with increasing in DHW or the occurrence of a coral bleaching event. Instead, it should increase only after the DHW rises or mass coral bleaching events occur. This phenomenon can indeed be observed in Fig. 11.

Quantitatively, we further calculated the average DHW over six months before and after each day and performed a correlation analysis with RCLs for different lag times. Here, all the RCLs shown in Fig. 6 were used. As shown in Fig. 12, the peak correlation occurred at lag times between 1.4 and 2.1 years, with correlation coefficients ranging from 0.58 to 0.60. Furthermore, we correlated the DHWs with the RCLs for each coral reef that exhibited more than 5 RCLs. The results revealed that the maximum correlation coefficients for the reefs ranged from 0.56 to 0.91, with lag times ranging from 1.4 to 2.3 years.

4.3. Limitations of the proposed methods and corresponding potential solutions

In this study, the focus was only on coral islands and reefs in the South China Sea (SCS), but the proposed method has great potential for application to other coral reefs. First, the proposed method requires dividing a year into a few-competitive-alga period and a lush-competitive-alga period. For the SCS, the few-competitive-alga period and the lush-competitive-alga period refer specifically to January–March and April–October, respectively. However, these periods may differ in other regions. One solution is to 1) apply T^{F}_{NRGI} to each image in a year and select the set with the minimal area as the set of live-coral growth pixels and 2) similarly apply T^{L}_{NRGI} to each image in the same year and select the set with the maximal area as the set of the live-coral-or-competitive-algae growth pixels. Another simpler solution is to redefine the few-competitive-alga period and the lush-competitive-alga period for a specific region. For example, as shown in Fig. 13, we can obtain the live-coral growth zone area, the competitive-algae growth zone area, and the RCL of a coral reef in the southern Great Barrier Reef

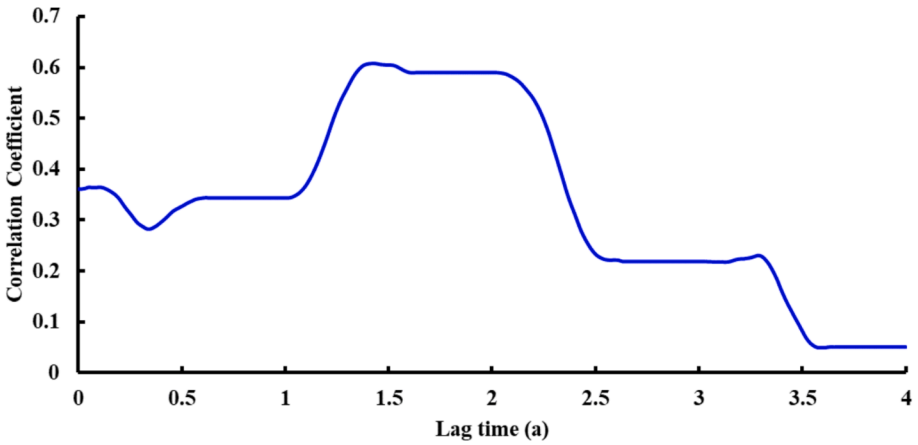

Fig. 12. Correlations between the DHWs and the RCLs for different lag times.

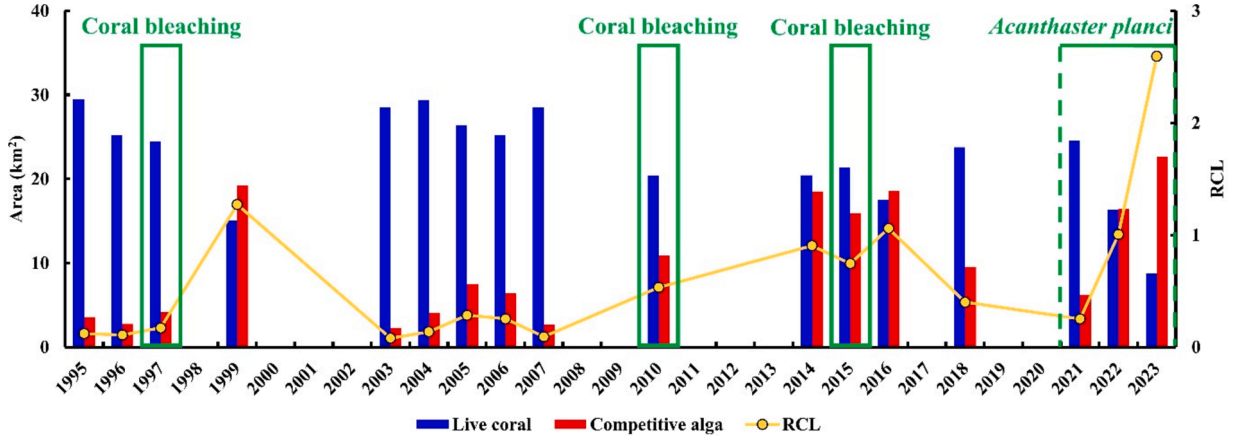

Fig. 13. Comparisons of typical coral bleaching (Berkelmans and Oliver, 1999; Tan et al., 2018; Bainbridge, 2017) and Acanthaster planci outbreak events (Matthews et al., 2024) with the characteristics of the live coral and competitive algae growth zones of a coral reef in the southern Great Barrier Reef.

(Supporting Information, Fig. S12) by redefining the few-competitive-alga period and lush-competitive-alga period as June–September and November–February, respectively. The variations in the growth zone characteristics of the live corals and competitive algae are also quite consistent with the mass coral bleaching events and the outbreak of *Acanthaster planci* in the southern Great Barrier Reef.

Cloud cover and limited image availability can restrict the temporal resolution of analyses via the proposed method, particularly in early years. Fortunately, with the increasing number of remote sensing satellites being launched worldwide, the interval between satellite observations of coral reefs is decreasing. For example, the joint use of Landsat 8 and Landsat 9 reduces the interval to 8 days, while the joint use of Sentinel-2A and Sentinel-2B reduce it to 5 days. Correspondingly, this increased frequency allows for more opportunities to select enough appropriate images to meet the multitemporal satellite image requirements of the proposed approach, even in tropical and subtropical regions where coral reefs are often located, and cloudy or rainy weather is common. Therefore, we believe that the proposed approach has a promising application prospects for future coral reef monitoring.

In addition, some studies have highlighted that ecological changes in coral reefs are related to certain oceanic conditions. For example, Yao and Wang (2022) reported that severe marine heatwaves (MHWs) induced higher rates of coral bleaching, with more than 25 % coral bleaching occurring when the total days of MHW exceeded 60 days during strong El Niño years. This study provides time series data for the live-coral growth zone area, competitive-algae growth zone area, and RCL, which can indicate the dynamic status of a coral reef ecosystem. In the future, we aim to fuse these time series data with other datasets, such as oceanographic data, sea surface temperature (SST), marine cold-spell (MCS), and MHW data, to gain a more comprehensive understanding of coral reef dynamic changes and their relationships with oceanic conditions.

5. Conclusions

To address the challenge of different objects having similar spectra in multispectral satellite images for assessing coral reef ecosystems, we leveraged the fact that competitive algae undergo seasonal dieback, whereas live-coral growth zones remain relatively stable over short periods. Rather than striving for higher classification accuracy for live-coral and competitive-algae growth zones via a single satellite image, we utilized two images taken at different times: one during the few-competitive-alga period and another during the lush-competitive-alga period (from Landsat TM/OLI or Sentinel-2 MSI). This method allowed us to assess the characteristics of the live-coral and competitive-algae growth zones (including both areas of both zones and the RCL).

Our approach is straightforward. First, we proposed the *NRGI* to segment live-coral-or-competitive-algae growth zones in two satellite images separately. Then, we estimated the growth zone characteristics by analysing the differences between the segmentation results from the few-competitive-alga period image and the lush-competitive-alga period image. The experimental results for eight typical coral islands and reefs in the SCS demonstrated the effectiveness and feasibility of the proposed method. The derived growth zone characteristics (live-coral growth

zone area, competitive-algae growth zone area, and RCL) are crucial for determining the status of a coral reef ecosystem.

Intuitively, the varying trends of the live-coral and competitive-algae growth zone characteristics were consistent with major ecological disaster events and coral reef recovery periods. Quantitatively, the RCL was well correlated with the coral-macroalgae encounter rate, and a time-lagged correlation was observed between heat stress (DHW) and the RCL. Therefore, the proposed growth zone characteristics of live corals and competitive algae can serve as feasible and effective indices for assessing the status of a coral reef ecosystem, such as the pressure of competitive algae on live corals and the extent of degradation of coral reef ecosystems caused by mass coral bleaching or mortality events.

In addition to providing historical dynamic information about coral reef ecosystems, we believe that the proposed approach has significant potential for future coral reef monitoring. This study offers valuable insights into the dynamic changes in coral reef ecosystems and provides a crucial basis for integrating remote sensing technology and coral reef ecology.

CRediT authorship contribution statement

Rongyong Huang: Writing – review & editing, Writing – original draft, Methodology, Investigation, Conceptualization. **Zhiwei He:** Writing – review & editing, Writing – original draft, Methodology, Conceptualization. **Kefu Yu:** Methodology, Investigation, Conceptualization. **Zuofang Yao:** Formal analysis. **Bin Zou:** Formal analysis. **Junyou Xiao:** Formal analysis.

Declaration of competing interest

The authors declare that they have no known competing financial interests or personal relationships that could have appeared to influence the work reported in this paper.

Data availability

The Landsat images can be downloaded from the United States Geological Survey (USGS) (https://earthexplorer.usgs.gov/), and the Sentinel-2 MSI images were downloaded from the Copernicus Data Space Ecosystem of the European Space Agency (ESA) (https://dataspace.copernicus.eu/). The live coral cover (LCC) and competitive alga cover (CAC) data can be obtained from the National Earth System Science Data Center, National Science & Technology Infrastructure of China (http://www.geodata.cn) and the following two documents: Chen, X., Yu, K., Huang, X., Wang, Y., Liao, Z., Zhang, R., Yao, Q., Wang, J., Wang, W., Tao, S., & Zhang, H., 2019. Atmospheric Nitrogen Deposition Increases the Possibility of Macroalgal Dominance on Remote Coral Reefs. J. Geophys. Res. Biogeosciences 124, 1355–1369. https://doi.org/10.1029/2019JG005074. Liao, Z., Yu, K., Chen, B., Huang, X., Qin, Z., & Yu, X., 2021. Spatial distribution of benthic algae in the South China Sea: Responses to gradually changing environmental factors and ecological impacts on coral communities. Divers. Distrib. 27, 929–943. https://doi.org/10.1111/ddi.13243. Other data that support the findings of this study are available from the corresponding author upon reasonable request.

Acknowledgments

This work was supported by National Natural Science Foundation of China (Nos. 42090041, 42030502), Key Research and Development Project of Hainan Province (No. ZDYF2024SHFZ086), National Natural Science Foundation of China (No. 41766007). Special thanks are given to the anonymous reviewers and members of the editorial board for their suggestions of improving this article. We also thank the team of Prof. Zuxun Zhang at the School of Remote Sensing Information Engineering, Wuhan University, the Nansha Islands Coral Reef Ecosystem National Observation and Research Station, and Dr. Honglei Jiang in School of Marine Sciences, Guangxi University for their suggestions on improving this article.

Appendix A. Supplementary data

Supplementary data to this article can be found online at https://doi.org/10.1016/j.jag.2024.104194.

References

Bainbridge, S.J., 2017. Temperature and light patterns at four reefs along the Great Barrier Reef during the 2015–2016 austral summer: understanding patterns of observed coral bleaching. J. Oper. Oceanogr. 10, 16–29. https://doi.org/10.1080/1755876X.2017.1290863.

Berkelmans, R., Oliver, J.K., 1999. Large-scale bleaching of corals on the Great Barrier Reef. Coral Reefs 18, 55–60. https://doi.org/10.1007/S003380050154.

Birrell, C.L., McCook, L.J., Willis, B.L., 2005. Effects of algal turfs and sediment on coral settlement. Mar. Pollut. Bull. 51, 408–414. https://doi.org/10.1016/j.marpolbul.2004.10.022.

Chen, Q., Deng, R., Qin, Y., Xiong, L., He, Y., 2015. Analysis of spectral characteristics of coral under different growth patterns. Acta Ecologica Sinica. 35, 3394–3402. https://doi.org/10.5846/stxb201306261783.

Chen, X., Yu, K., Huang, X., Wang, Y., Liao, Z., Zhang, R., Yao, Q., Wang, J., Wang, W., Tao, S., Zhang, H., 2019. Atmospheric nitrogen deposition increases the possibility of macroalgal dominance on remote coral reefs. J. Geophys. Res. Biogeosciences 124, 1355–1369. https://doi.org/10.1029/2019JG005074.

De'Ath, G., Fabricius, K.E., Sweatman, H., Puotinen, M., 2012. The 27-year decline of coral cover on the Great Barrier Reef and its causes. Proc. Natl. Acad. Sci. USA 109 (44), 17995–17999. https://doi.org/10.1073/pnas.1208909109.

Duan, Z., 2022. Evaluation of coral reef ecological resistance in xisha islands based on remote sensing technology. Guangxi Univ, Nanning, China. M.S. Thesis.

Ferrari, R., Gonzalez-Rivero, M., Ortiz, J.C., Mumby, P.J., 2012. Interaction of herbivory and seasonality on the dynamics of Caribbean macroalgae. Coral Reefs 31, 683–692. https://doi.org/10.1007/s00338-012-0889-9.

Fitt, W.K., McFarland, F.K., Warner, M.E., Chilcoat, G.C., 2000. Seasonal patterns of tissue biomass and densities of symbiotic dinoflagellates in reef corals and relation to coral bleaching. Limnol. Oceanogr. 45, 677–685. https://doi.org/10.4319/LO.2000.45.3.0677.

Fricke, A., Teichberg, M., Beilfuss, S., Bischof, K., 2011. Succession patterns in algal turf vegetation on a Caribbean coral reef. Botanica Marina 54, 111–126. https://doi.org/10.1515/bot.2011.021.

Gardner, T.A., Côté, I.M., Gill, J.A., Grant, A., Watkinson, A.R., 2003. Long-term region-wide declines in Caribbean corals. Science 301 (5635), 958–960. https://doi.org/10.1126/science.1086050.

Hochberg, E.J., Atkinson, M.J., 2003. Capabilities of remote sensors to classify coral, algae, and sand as pure and mixed spectra. Remote Sens. Environ. 85, 174–189. https://doi.org/10.1016/S0034-4257(02)00202-X.

Huang, H., You, F., Lian, J., Yang, J., Li, X., Dong, Z., Zhang, C., Yuan, T., 2011. Species diversity and distribution of scleractinian coral at Xisha Islands, China. Biodivers. Sci. 19, 710–715. https://doi.org/10.3724/SP.J.1003.2011.06132.

Huang, L., Yu, K., 2010. Review on coral disease: types, ecological influences and the relationships with environmental factors. Acta Ecologica Sinica 30 (5), 1328–1340.

Huang, R., Yu, K., Wang, Y., Wang, W., Mu, L., Wang, J., 2018. Method to design a live coral cover sensitive index for multispectral satellite images. Opt. Express 26, A374. https://doi.org/10.1364/OE.26.00A374.

Huang, R., Yu, K., Wang, Y., Liu, J., Zhang, H., 2019. Progress of the study on coral reef remote sensing. J. Remote Sens. 23, 1091–1112. https://doi.org/10.11834/jrs.20198110.

Leiper, I., Phinn, S., Dekker, A.G., 2011. Spectral reflectance of coral reef benthos and substrate assemblages on Heron Reef, Australia. Int. J. Remote Sensing 33 (12), 3946–3965. https://doi.org/10.1080/01431161.2011.637675.

Li, Y., Wu, Z., Liang, J., Chen, S., Zhao, J., 2019a. Analysis on the outbreak period and cause of Acanthaster planci in Xisha Islands in recent 15 years (in Chinese). Chin. Sci Bull. 64, 3478–3484. https://doi.org/10.1360/TB-2019-0152.

Li, Y., Liang, J., Wu, Z., Chen, S., 2019b. Outbreak and Prevention of Acanthaster planci. Ocean Devel. Manag. 36, 9–12. https://doi.org/10.20016/j.cnki.hykfygl.2019.08.002.

Li, S., Yu, K., Chen, T., Shi, Q., Chen, T., 2011a. Seasonal patterns of densities of symbiotic zooxanthellae in scleractinian corals from Daya Bay, northern South China Sea, and relation to coral bleaching. J. Tropical Oceanography 30, 39–45. https://doi.org/10.3969/j.issn.1009-5470.2011.02.006.

Li, S., Yu, K., Chen, T., Shi, Q., Zhang, H., 2011b. Assessment of coral bleaching using symbiotic zooxanthellae density and satellite remote sensing data in the Nansha Islands, South China Sea. Chin. Sci Bull 56, 747–755. https://doi.org/10.1007/s11434-011-4390-6.

Liao, Z., Yu, K., Wang, Y., 2016. Review on the effect of macroalgae on the degeneration of coral reefs. Acta Ecologica Sinica 36, 6687–6695. https://doi.org/10.5846/stxb201505040909.

Liao, Z., Yu, K., Chen, B., Huang, X., Qin, Z., Yu, X., 2021. Spatial distribution of benthic algae in the South China Sea: Responses to gradually changing environmental factors and ecological impacts on coral communities. Divers. Distrib. 27, 929–943. https://doi.org/10.1111/ddi.13243.

Low, J.K.Y., Fong, J., Todd, P.A., Chou, L.M., Bauman, A.G., 2019. Seasonal variation of Sargassum ilicifolium (Phaeophyceae) growth on equatorial coral reefs. J. Phycol. 55, 289–296. https://doi.org/10.1111/JPY.12818.

Luo, H., 2019. The distribution characteristics of turf algae and its potential effect on scleractinian coral in the reefs of mid-northern south china sea. Guangxi Univ, Nanning, China. M.S. Thesis.

Madin, J.S., Madin, E.M.P., 2015. The full extent of the global coral reef crisis. Conserv. Biol. 29, 1724–1726. https://doi.org/10.1111/COBI.12564.

Matthews, S., Williamson, D., Beeden, R., 2024. Protecting Great Barrier Reef resilience through effective management of crown-of-thorns starfish outbreaks. Plos One 19 (4), e0298073.

McCook, L.J., 2001. Competition between corals and algal turfs along a gradient of terrestrial influence in the nearshore central Great Barrier Reef. Coral Reefs 19, 419–425. https://doi.org/10.1007/S003380000119/METRICS.

McField, M., Soto, M., Craig, N., Giro, A., Drysdale, I., Guerrero, C., Rueda, M., Kramer, P., Canty, S., Muñiz, I., 2022. Mesoamerican Reef Report Card. Healthy Reefs Initiative. www.healthyreefs.org.

McManus, J.W., Polsenberg, J.F., 2004. Coral–algal phase shifts on coral reefs: Ecological and environmental aspects. Prog. Oceanogr. 60, 263–279. https://doi.org/10.1016/J.POCEAN.2004.02.014.

Moberg, F., Folke, C., 1999. Ecological goods and services of coral reef ecosystems. Ecol. Econ. 29, 215–233. https://doi.org/10.1016/S0921-8009(99)00009-9.

Mumby, P.J., Edwards, A.J., 2002. Mapping marine environments with IKONOS imagery: enhanced spatial resolution can deliver greater thematic accuracy. Remote Sens. Environ. 82, 248–257. https://doi.org/10.1016/S0034-4257(02)00041-X.

Raymundo, L.J., Maypa, A.P., 2002. Recovery of the Apo Island Marine Reserve, Philippines, 2 years after the El Niño bleaching event. Coral Reefs 21, 260–261. https://doi.org/10.1007/s00338-002-0237-6.

Riegl, B., Piller, W.E., 2003. Possible refugia for reefs in times of environmental stress. Int. J. Earth Sciences 92, 520–531. https://doi.org/10.1007/S00531-003-0328-9.

River, G.F., Edmunds, P.J., 2001. Mechanisms of interaction between macroalgae and scleractinians on a coral reef in Jamaica. J. Exp. Mar. Biol. Ecol. 261, 159–172. https://doi.org/10.1016/S0022-0981(01)00266-0.

Roff, G., 2020. Reef accretion and coral growth rates are decoupled in Holocene reef frameworks. Mar. Geol. 419, 106065. https://doi.org/10.1016/J.MARGEO.2019.106065.

Tan, C.H., Pratchett, M.S., Bay, L.K., Graham, E.M., Baird, A.H., 2018. Biennium horribile: very high mortality in the reef coral *Acropora millepora* on the Great Barrier Reef in 2009 and 2010. Mar. Ecol. Prog. Ser. 604, 133–142. https://doi.org/10.3354/meps12750.

Wabnitz, C.C., Andréfouët, S., Torres-Pulliza, D., Müller-Karger, F.E., Kramer, P.A., 2008. Regional-scale seagrass habitat mapping in the Wider Caribbean region using Landsat sensors: Applications to conservation and ecology. Remote Sens. Environ. 112, 3455–3467. https://doi.org/10.1016/J.RSE.2008.01.020.

Wilson, S.K., Robinson, J.P.W., Chong-Seng, K., Robinson, J., Graham, N.A.J., 2019. Boom and bust of keystone structure on coral reefs. Coral Reefs 38, 625–635. https://doi.org/10.1007/S00338-019-01818-4.

Wu, Z., Wang, D., Tu, Z., Li, Y., Chen, J., Zhang, G., 2011. The analysis on the reason of hermatypic coral degradation in Xisha. Haiyang Xuebao 33, 140–146.

Xu, J., Li, F., Meng, Q., Wang, F., 2019. The Analysis of Spectral Separability of Different Coral Reef Benthos and the Influence of Pigments on Coral Spectra Based on in Situ Data. Spectrosc. Spectr. Anal. 39, 2462–2469. https://doi.org/10.3964/j.issn.1000-0593(2019)08-2462-08.

Yang, H., Shen, J., Fu, F., Wang, Y., Zhao, N., 2014. Black band disease as a possible factor of the coral decline at the northern reef-flat of Yongxing Island, South China Sea. Sci. China: Earth Sci. 44, 642–653. https://doi.org/10.1007/s11430-013-4734-y.

Yao, Y., Wang, C., 2022. Marine heatwaves and cold-spells in global coral reef zones. Prog. Oceanography. 209, 102920. https://doi.org/10.1016/j.pocean.2022.102920.

Yu, K., 2012. Coral reefs in the South China Sea: Their response to and records on past environmental changes. Sci. China Earth Sci. 42, 1160–1172. https://doi.org/10.1007/s11430-012-4449-5.

Zeng, K., Xu, Z., Yang, Y., Zhang, Y., Zhou, W., Li, C., Huang, H., 2020. Design and Application of Reflectance Measurement System for Sea Bottom in Optically Shallow Water. Spectrosc. Spectr. Anal. 40, 579–585. https://doi.org/10.3964/j.issn.1000-0593(2020)02-0579-07.